HAL open science

The hidden brain-state dynamics of tACS aftereffects

Florian H Kasten, Christoph S Herrmann

To cite this version:

Florian H Kasten, Christoph S Herrmann. The hidden brain-state dynamics of tACS aftereffects. NeuroImage, 2022, 264, pp.119713. 10.1016/j.neuroimage.2022.119713 . hal-03842436

HAL Id: hal-03842436

https://hal.science/hal-03842436

Submitted on 7 Nov 2022

HAL is a multi-disciplinary open access archive for the deposit and dissemination of scientific research documents, whether they are published or not. The documents may come from teaching and research institutions in France or abroad, or from public or private research centers.

L'archive ouverte pluridisciplinaire **HAL**, est destinée au dépôt et à la diffusion de documents scientifiques de niveau recherche, publiés ou non, émanant des établissements d'enseignement et de recherche français ou étrangers, des laboratoires publics ou privés.

NeuroImage 264 (2022) 119713

Contents lists available at ScienceDirect

NeuroImage

journal homepage: www.elsevier.com/locate/neuroimage

The hidden brain-state dynamics of tACS aftereffects

Florian H. Kasten[a,b,c], Christoph S. Herrmann[a,d,*]

[a] Experimental Psychology Lab, Department of Psychology, European Medical School, Cluster of Excellence "Hearing4All", Carl von Ossietzky University, Oldenburg, Germany
[b] Centre de Recherche Cerveau & Cognition, CNRS, Toulouse, France
[c] Université Toulouse III Paul Sabatier, Toulouse, France
[d] Research Center Neurosensory Science, Carl von Ossietzky University, Oldenburg, Germany

ARTICLE INFO

Keywords:
Non-invasive brain stimulation
Brain-states
Transcranial alternating current stimulation
Brain oscillations
Aftereffects
Hidden Markov Models

ABSTRACT

Non-invasive techniques to electrically stimulate the brain such as transcranial direct and alternating current stimulation (tDCS/tACS) are increasingly used in human neuroscience and offer potential new avenues to treat brain disorders. Previous research has shown that stimulation effects may depend on brain-states. However, this work mostly focused on experimentally induced brain-states over the course of several minutes. Besides such global, long-term changes in brain-states, previous research suggests, that the brain is likely to spontaneously alternate between states in sub-second ranges, which is much closer to the time scale at which it is generally believed to operate. Here, we utilized Hidden Markov Models (HMM) to decompose magnetoencephalography data obtained before and after tACS into spontaneous, transient brain-states with distinct spatial, spectral and connectivity profiles. Only one out of four spontaneous brain-states, likely reflecting default mode network activity, showed evidence for an effect of tACS on the power of spontaneous α-oscillations. The identified state appears to disproportionally drive the overall (non-state resolved) tACS effect. No or only marginal effects were found in the remaining states. We found no evidence that tACS influenced the time spent in each state. Although stimulation was applied continuously, our results indicate that spontaneous brain-states and their underlying functional networks differ in their susceptibility to tACS. Global stimulation aftereffects may be disproportionally driven by distinct time periods during which the susceptible state is active. Our results may pave the ground for future work to understand which features make a specific brain-state susceptible to electrical stimulation.

1. Introduction

Non-invasive brain stimulation (NIBS) is increasingly used to assess the involvement of specific brain regions or activity patterns such as neural oscillations for certain cognitive functions. For example, an increasing body of research used interventional approaches to study the role of brain oscillations in cognition by means of rhythmic NIBS such as rhythmic transcranial magnetic stimulation (rTMS) and especially transcranial alternating current stimulation (tACS) (Bergmann and Hartwigsen, 2020; Herrmann et al., 2016b; Kasten and Herrmann, 2020; Klink et al., 2020; Vosskuhl et al., 2018). Apart from research applications, these techniques may offer new avenues for therapeutic interventions (Alexander et al., 2019; Elyamany et al., 2020; Mellin et al., 2018; Reinhart and Nguyen, 2019).

TACS works via the application of weak, alternating currents to the scalp and is believed to engage neural oscillations via entrainment (Fröhlich and McCormick, 2010; Herrmann et al., 2013; Johnson et al., 2020; Krause et al., 2019). On a physiological level, tACS has repeatedly been shown to alter human brain oscillations for several minutes or even beyond an hour after the offset of stimulation (Kasten et al., 2016; Neuling et al., 2013; Vossen et al., 2015; Zaehle et al., 2010). These aftereffects have been suggested to arise due to neural plasticity induced by the stimulation (Vossen et al., 2015; Wischnewski et al., 2019; Zaehle et al., 2010). In recent years, NIBS techniques received considerable criticism due to their weak and variable effects, leading some authors to question their efficacy altogether (Horvath et al., 2015a, 2015b; Lafon et al., 2017; Vöröslakos et al., 2018). It is suspected that a wide variety of individual factors may influence the effectiveness of NIBS (Ridding and Ziemann, 2010), including differences in brain anatomy (Kasten et al., 2019; Laakso et al., 2015) and genetic dispositions (Riddle et al., 2020). A number of studies further suggest, that effects of stimulation may depend on brain-states (Alagapan et al., 2016; Feurra et al., 2019, 2013; Neuling et al., 2013; Ruhnau et al., 2016). For example, tACS induced modulations in α-band activity were observed while participants kept their eyes open, but were absent when they kept their eyes closed (Alagapan et al., 2016; Neuling et al., 2013; Ruhnau et al., 2016). These observations were based on experimentally induced, comparably long-lasting changes in the brain's state. It is,

* Corresponding author at: Experimental Psychology Lab, Carl von Ossietzky University, Ammerländer Heerstr. 114 – 118, Oldenburg 26129, Germany.
E-mail address: christoph.herrmann@uni-oldenburg.de (C.S. Herrmann).

https://doi.org/10.1016/j.neuroimage.2022.119713.
Received 16 May 2022; Received in revised form 11 October 2022; Accepted 25 October 2022
Available online 26 October 2022.
1053-8119/© 2022 The Authors. Published by Elsevier Inc. This is an open access article under the CC BY license (http://creativecommons.org/licenses/by/4.0/)

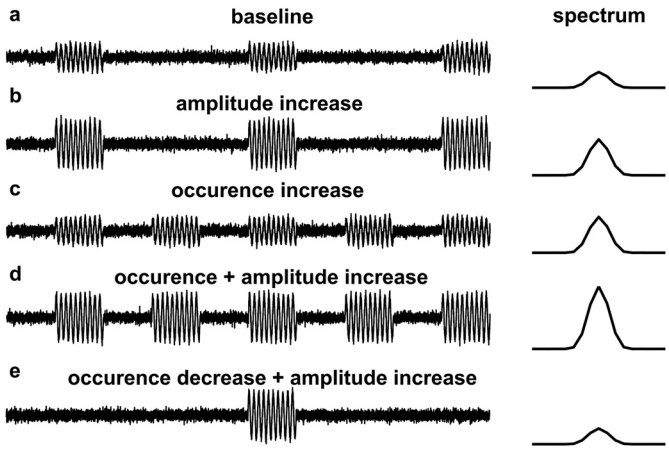

Fig. 1. *Possible activity changes underlying a tACS effect.* (a) Hypothetical M/EEG time series before stimulation. The activity pattern alternates between two states: short occurrences of 10 Hz α-activity and 'no-alpha' states. The resulting power spectrum is depicted on the right (b–d) After stimulation, an increase in the average power spectrum could potentially result from different changes in the activity pattern. (b) The amplitude in the alpha-state increases while the occurrence and time-spent in both states remain the same. (c) The time spent in the α-state increases, while the time spent in the 'no-alpha' state decreases. The amplitude of the oscillation remains the same. (d) Both the time-spent in the α-state and the amplitude of the oscillation change. (e) The amplitude of the oscillation increases, while the occurrence of the α-state decreases. In this scenario, the effect of tACS on oscillatory power might be obscured by the change of state occurrence.

however, likely that even under relatively constant experimental conditions, the brain spontaneously alternates between different, transient states at rates of a few seconds or even at sub-second ranges, rather than remaining in a constant state (Baker et al., 2014; Vidaurre et al., 2018b). Recent work underpins this idea and demonstrated that such transient states exhibit distinct patterns of oscillatory activity and connectivity (Vidaurre et al., 2016, 2018b). It is thus tempting to assume that these 'hidden', spontaneous brain-states may also differ in their susceptibility to the same brain stimulation protocol. Such a phenomenon would bring about certain issues for the analysis of stimulation effects. A change in oscillatory power over a longer period of time can in principle occur in multiple ways. It is usually assumed that the effect of tACS results from an increase in the amplitude of the target oscillation (Fig. 1 a, b). However, it is also possible that changes in spectral power arise from a more frequent occurrence of brain-states with comparably higher oscillatory power, without necessarily changing the actual amplitude of oscillations within each state (Quinn et al., 2019) (Fig. 1c). Alternatively, stimulation effects may be obscured if an increase in power in a given state is accompanied by a reduced occurrence of the state or vice versa (Fig. 1e).

The goal of the current study is to establish if differential effects of tACS on transient brain-states as outlined above exist, and to dissociate effects of tACS on oscillatory power from those on the occurrence of oscillatory activity. The existence of such transient brain-state dynamics would open a whole new perspective on tACS and brain stimulation data in general. In order to achieve our objectives, we adapted a recently proposed analysis pipeline utilizing Hidden Markov Models (HMMs) to decompose neural time-series data into distinct, transient brain-states (Baker et al., 2014; Vidaurre et al., 2016, 2018b). The analysis was carried out on two recently obtained tACS-magnetoencephalography (MEG) datasets (Kasten et al., 2019). Due to the nature of the available data, we cannot yet resolve the intricacies of such transient brain-state dynamics, which, among other things, pertains the role of the frequency band or montage with which tACS is applied. We hypothesized that occipito-parietal α-tACS differentially affects power in the α-band across brain-states but does not alter the relative time spent in each state.

2. Methods

2.1. Participants

All analyses in the current study were conducted on two pre-existing tACS-MEG datasets (Kasten et al., 2019). The first one was carried out as a single-blind, between subject design on 40 participants (24 ± 3 years, 20 females) with participants randomly assigned to one out of two experimental groups (tACS vs. sham), while counterbalancing for participants' sex. The second experiment was performed as a single-blind within-subject design ($N = 19$, 25 ± 3 years, 11 females), with participants receiving both stimulation conditions at random order across two experimental sessions scheduled on two separate days. Participants were right-handed according to the Edinburgh Handedness-Inventory (Oldfield, 1971), had normal or corrected-to-normal vision, were non-smokers, without history of neurological or psychiatric disease and medication-free at the day of the experiment. Written informed consent was obtained from all subjects, both experiments were approved by the Commission for Research Impact assessment and Ethics at the University of Oldenburg and complied with all relevant ethical regulations.

2.2. Magnetoencephalogram (MEG)

MEG signals were obtained at a rate of 1 kHz using a 306-channel whole-head MEG system (Elekta Neuromag Triux System, Elekta Oy, Helsinki, Finland) inside a magnetically shielded room (MSR; Vacuumschmelze, Hanau, Germany). Participants' head-position was continuously monitored using five head-position indicator (HPI) coils, attached to participants' heads. Positions of the coils were digitized along with participants' head shapes with a Polhemus Fastrak (Polhemus, Colchester, VT, USA) for later co-registration with structural MRIs (T1-weighted 3D sequence, MPRANGE, TR = 2000 ms, TE = 2.07 ms, slice thickness: 0.75 mm; Siemens Magnetom Prisma 3 T MRI machine, Siemens, Erlangen, Germany).

2.3. Electrical stimulation

TACS was administered via two surface-conductive rubber electrodes positioned over locations Cz (7 × 5 cm) and Oz (4 × 4 cm) of the international 10-10 system via an electrically conductive, adhesive paste (ten20 paste, Weaver & Co, Aurora, CO, USA). The stimulation waveform was generated using a constant current stimulator (DC Stimulator Plus, Neuroconn, Illmenau, Germany) and remote-controlled via a digital-to-analog converter (NI-USB 6251, National Instruments, Austin, TX, USA) fed with data by a MATLAB script (MATLAB 2016a, The Math Works Inc., Natick, MA, USA). Stimulation currents were guided into the MSR via the MRI extension-kit of the stimulator. Impedances were kept below 20 kΩ, including two 5 kΩ resistors inside the stimulation cables. Participants received 20 min of active tACS or sham stimulation (30 s of tACS at the beginning of the stimulation period) at their individual α-frequency (IAF). IAF was determined from a 3 min resting MEG obtained prior to the main experiment. 10 min of MEG were recorded directly before and after stimulation. To ensure participants remained attentive and kept their eyes open during the recording, they were asked to perform a simple visual change detection task. To this end, a white fixation-cross on gray background was rear-projected onto a screen (distance: ~100 cm) inside the MSR. Participants had to manually respond to a 500 ms rotation of the cross by 45°, occurring at random intervals with a stimulus onset asynchrony of 10–110 s. Additional details on the experimental procedures, including debriefing and the assessment of adverse effects can be found in a previous publication on the data (Kasten et al., 2019).

2.4. Data analysis

2.4.1. Preprocessing

MEG preprocessing was performed in MATLAB 2019b using the fieldtrip toolbox (Oostenveld et al., 2011). HMM training and state-wise frequency analysis was performed using the HMM-MAR toolbox (https://github.com/OHBA-analysis/HMM-MAR). Statistical analysis was carried out in R 3.6.1 (The R Core Team, Vienna, Austria) running on R-Studio (RStudio Team, PBC, Boston, MA, USA). Statistical functions provided by the fieldtrip toolbox were utilized to compute cluster-permutation statistics (Maris and Oostenveld, 2007).

In a first step, spatio-temporal signal-space-seperation (tSSS) was applied to the data to suppress external interferences and correct for head-movements during the recording (Nenonen et al., 2012; Taulu et al., 2005; Taulu and Simola, 2006). TSSS was applied using MaxFilter™ v2.2 (Elekta Neuromag Oy, Helsinki, Finland) with standard settings (L_{in} = 8, L_{out} = 3, correlation limit = .98). Signals were subsequently imported to MATLAB. To reduce computational demands, the analysis was exclusively performed on the 102 magnetometer channels. Signals were resampled to 256 Hz and filtered between 1 and 40 Hz using 6th-order forward-backward Butterworth filters. An independent component analysis (ICA) was performed to remove signal components reflecting eye-movements, cardiac artifacts and stimulator noise. MEG time-series were then projected into source-space using an LCMV beamformer (Van Veen et al., 1997) with single-shell head models (Nolte, 2003) and a 10 mm source-grid warped into Montreal Neurological Institute (MNI) space. Source time series were subsequently parcellated into 42 virtual channels representing the activity of cortical regions of interest (ROIs) covering the entire cortex. The regions correspond to the ROIs used in Vidaurre et al. (2018b). A weight-matrix was used to project data into brain-space for visualization purposes. A multivariate correction for spatial-leakage (Colclough et al., 2015) was applied using the ROInets toolbox (https://github.com/OHBA-analysis/MEG-ROI-nets). The correction reduces artificial correlations between adjacent virtual channels, while resembling the original data as close as possible. Such correlations are known to bias connectivity estimates and can hamper HMM training. A conceptual overview of the analysis pipeline is provided in Fig. 2.

2.4.2. Hidden Markov Model

HMMs are used to infer a sequence of a finite number of hidden states of a system, based on their observable emissions (e.g., patterns of measurable brain signals), where each state has a certain probability to be accompanied by each emission. It is assumed that at each timepoint t, the system is in one out of K discrete states and that the observable data o at each timepoint is drawn from an observation distribution, which is of the same family in all states. However, for each state the observation model has a different set of parameters (e.g., different mean and/or SD for a Gaussian observation model) (Vidaurre et al., 2018b). The transition probability between states is Markovian, i.e., it depends exclusively on the previous state s_{t-1}:

$$P(s_t|s_1 \dots s_{t-1}) = P(s_t|s_{t-1}) = \pi_t$$

where π_t is the (K x K) transition probability matrix, containing the transition probability between all states. The standard approach for training an HMM with a fixed number of states and unknown transition and emission probabilities is the Baum-Welch algorithm – also referred to as the Forward-Backward algorithm (Baum et al., 1970). The algorithm estimates both the emission and transition probabilities by starting off with an initial estimate and then iteratively optimizing both probability matrices. As this requires a complete sequential forward- and backward pass through the entire concatenated data of all subjects, which is demanding in terms of memory usage and computation times, we opted to run the algorithm with a recently developed stochastic inference procedure implemented in the HMM-MAR toolbox. In contrast, to traditional approaches using variational inference or maximum likelihood, stochastic inference allows to perform HMM training on large datasets

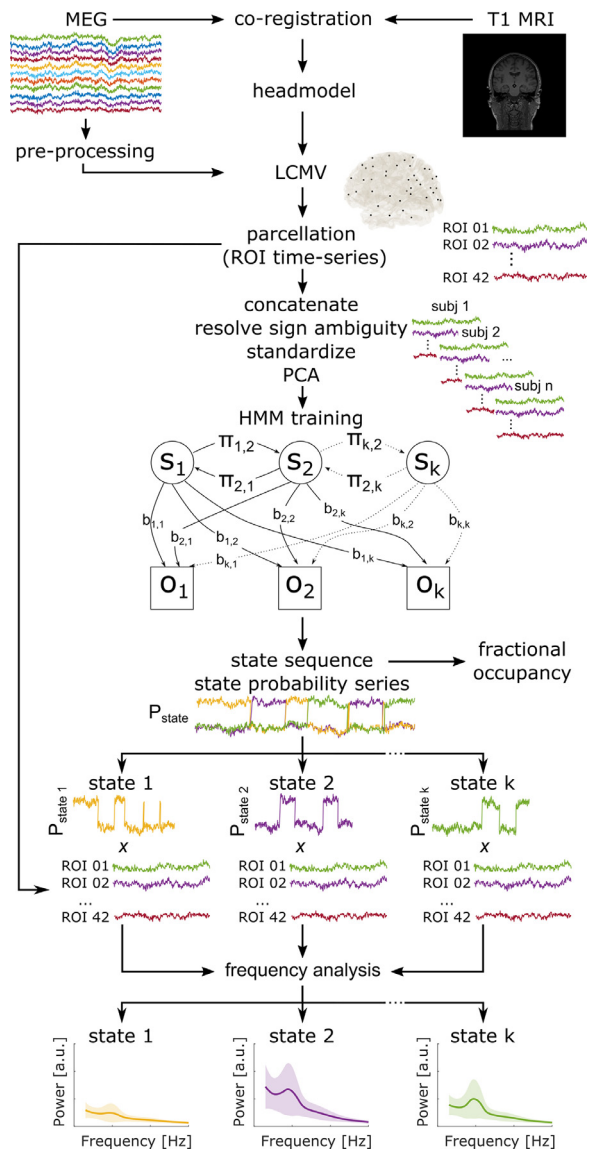

Fig. 2. *Analysis Pipeline*. Preprocessed MEG signals were projected into source-space using an LCMV beamformer. Source time-series were parcellated into 42 ROIs. Before HMM training, single-subject time-series were concatenated, differences in dipole signs across subjects were resolved and the data was standardized within subjects to avoid the HMM to adapt to inter-individual differences. The HMM was then trained on the data in PCA space (84 components). The HMM infers a sequence of a finite number of hidden states (s_1, …, s_k) based on a set of observable emissions (o_1, …, o_k). Emissions and states are linked via an emission probability matrix b, where each state has a probability to cause each emission. The transition probability between states is represented in the transition probability matrix π. Both matrices are unknown and need to be estimated from the data by an iterative algorithm (e.g. Baum-Welch). The HMM returns the most likely sequence of states, which are used to compute the relative time spent in each state (a.k.a. fractional occupancy), as well as the underlying state probability series. For each timepoint, the series contains a probability of each state being active. By weighting the ROI time series with the state probability series, state-wise frequency spectra and connectivity measures can be computed.

at reasonable memory requirements and computation times, by estimating interim state observation models on computationally more efficient subsets of data (Vidaurre et al., 2018a). Due to the additive nature of Gaussian distributions, these can be linearly combined to update the HMM observation model (for details on the stochastic inference procedure please refer to Vidaurre et al. 2018a). In line with previous work, we ran stochastic inference with a batch size of M = 5. Once the tran-

sition and emission probabilities are estimated, a state probability sequence γ, indicating the probability of each state being active at each timepoint, can be computed along with the most likely state sequence (Fig. 2). These form the basis for subsequent analyses characterizing each state's relative occurrence, dwell time and switching rate, as well as it is frequency content (see next section).

We followed the analysis framework described by Vidaurre et al. (2018b) using a time-delay-embedded HMM (TDE-HMM) trained on the concatenated ROI time series of all participants. This variant of the HMM, uses a Gaussian observation model with zero mean to model the data over a certain time window, effectively utilizing the data autocovariance across regions. The TDE-HMM is sensitive to changes in power and phase-locking while being able to deal with a relatively large number of channels (Vidaurre et al., 2018b). We chose a TDE-HMM with an observation window of 15 samples centered around each t and working in PCA-space with 84 components (explaining ~68% of the variance in both datasets). This forces the model to return a common set of states across the whole dataset. To avoid that the model assigns states based on inter-individual differences between subjects, ROI time-series were standardized (z-transformed) within each subject and the dipole-sign-ambiguity of individual time-series was resolved using the approach presented in Vidaurre et al. (2018b). After the training, we visually confirmed that each state was present in each subject (Supplementary Figs. 1 and 2). The underlying MATLAB code for HMM training and state-wise frequency analysis (see next section) can be obtained via the open science framework (see section Data availability).

A common challenge in the application of HMMs, particularly to biological data, is the definition of the number of states for the model, which has to be pre-specified by the user. Objective model selection procedures, e.g., based on Akaike's or Bayesian Information Criterion (AIC, BIC), or the comparison of free energy (Baker et al., 2014), have been proposed for the selection of model complexity. However, these approaches often favor models with large numbers of states that are difficult to handle and interpret (Pohle et al., 2017). It is thus suggested to take a more practical approach integrating objective measures with practical considerations such as interpretability of results and usefulness in the light of the research question (Pohle et al., 2017). For our analysis we considered eleven different HMMs with the max number of states ranging from 2 to 12. Indeed, the free energy for these HMMs monotonically decreased from the 2- to the 12-state HMM (Supplementary Fig. 3). However, two "knees" in the trajectory indicate that after including state 4, additional states have less impact on free energy as compared to the previous states. In addition, HMMs with larger numbers of states tended to return states that are similar with respect to their spatial and spectral patterns (e.g., the 6-state HMM, Supplementary Fig. 4), indicating that a state may have been split into sub-states with only minor differences, which is undesirable for our analysis. Based on these considerations we decided to settle for a 4-state HMM for subsequent analyses.

2.4.3. Fractional occupancy and state-wise frequency analysis

After HMM training, we utilized the obtained probabilistic state sequence to compute fractional occupancy, i.e., the relative time each subject spent in each state, during the baseline and post-stimulation blocks, respectively. To this end, each time-point was assigned to the most probable state and the proportion of time points relative to the total amount of time points per subject and block was computed for each state. In addition, we extracted each states' so-called dwell and interval times, referring to the average duration of a state visit and the average time between two visits to the same state, respectively. Although these characteristics of the states cannot readily explain changes in overall spectral power, as the state occupancy can, they do allow to characterize the temporal progression of the states.

In order to obtain state-wise frequency and connectivity profiles, we leveraged the probabilistic state-time course to perform a state-wise multi-taper analysis (Fig. 2, bottom) (Vidaurre et al., 2016). The standard multi-taper power spectral density (PSD) of the entire time series is given by $|S(f)|^2$, with

$$S(f) = \frac{1}{\sqrt{R}} \sum_{r=1}^{R} \sum_{t=1}^{T} \delta_t^{(r)} y_t e^{-2\pi i f t}$$

where $\delta_t^{(r)}$ is the value of the rth taper at time point t. To obtain a state-wise spectral analysis for each of the k states, the data y at each time point t is weighted by the probability of being in that state ρ, such that the PSD for the kth state can be obtained by:

$$S(f) = \frac{1}{\sqrt{R}} \sum_{r=1}^{R} \sum_{t=1}^{T} \rho_t^{(k)} \delta_t^{(r)} y_t e^{-2\pi i f t}$$

with

$$\rho_t^{(k)} = \frac{\sqrt{\gamma_t^{(k)}}}{\sqrt{\sum_{t=1}^{T} \gamma_t^{(k)} / T}}$$

where the normalization term for $\rho_t^{(k)}$ is chosen to preserve the total power of the signal, i.e. the sum of the state spectra (weighted by the state probability) corresponds to the total spectrum of the signal (Vidaurre et al., 2016). From these PSD estimates, measures of connectivity, such as coherence can be computed.

State-wise PSD and coherence were computed separately for the baseline and post-stimulation blocks using Slepian sequences with 7 tapers and a time-bandwidth product of 4. Importantly, we used the unstandardized ROI time-series for the analysis as the standardization can cancel out differences between blocks and subjects (i.e., stimulation effects). For inspection of the states' overall spectral, spatial and connectivity profiles, results were averaged across recording blocks and subjects, after re-aligning individual spectra on the IAF. For statistical analysis, PSD in each recording block was averaged within the individual α-band (IAF ± 2 Hz). To facilitate statistical comparisons, the relative change in IAF band power after stimulation relative to baseline was computed:

$$rel.\ change = \frac{A - B}{B}$$

where A is IAF band power after tACS or sham stimulation, and B is IAF band power in the baseline recording. To test if effects on state power are specific to the α-frequency range, we repeated the analysis for the neighboring individual θ- (IAF-7 Hz – IAF-3 Hz) and β-band (IAF + 4 Hz – IAF + 20 Hz). It should be noted that, while this control analysis can serve to assess if the response to α-tACS is specific to the α-band, it does not allow to determine if the response in the α-band is specific to α-tACS (or of similar effects could be achieved by stimulation in other frequency bands). The latter would require the inclusion of additional stimulation frequency conditions, which are not available for the current dataset.

In addition, we ran the frequency analysis on the ROI time series without weighting by states to test for non-state resolved effects of tACS in the second dataset. This allows to compare tACS effects within states, to those commonly seen on the global level.

2.4.4. Resolving the contribution of states to the global stimulation effect

In order to assess the contribution of each state to the global stimulation effect, we developed an undirected and a directed state contribution index (SCI). As described in the previous section, state-wise power spectra can be computed by weighting the ROI time series with the state probability series. Their sum weighted by the state probability γ should resemble the total power of the original signal:

$$PSD_{total} = \sum_{k=1}^{K} PSD_k \frac{\sum_{t=1}^{T} \gamma_{t,k}}{T}$$

Based on this rationale, we can compute an index of the contribution of each state to the overall dynamics of the global tACS effect, by taking

the absolute value of the state-wise effect of the kth state and dividing it by the sum of the absolute value of all effects:

$$SCI_{undirected} = \frac{\left|Effect^{(k)}\right|}{\sum_{k=1}^{K} |Effect_k|}$$

where the effect is defined as the difference in power change from pre- to post-stimulation between the tACS and the sham condition within each state after weighting each PSD estimate with the average probability of the state within the specific experimental block.

$$Effect^{(k)} = \left(PSD^{(k)}_{post,tACS}\,\gamma^{(k)}_{post,tACS} - PSD^{(k)}_{pre,tACS}\,\gamma^{(k)}_{pre,tACS}\right) - \left(PSD^{(k)}_{post,sham}\,\gamma^{(k)}_{post,sham} - PSD^{(k)}_{pre,sham}\,\gamma^{(k)}_{pre,sham}\right)$$

The undirected SCI provides an estimate of the relative contribution of each state to the overall dynamics across all states. By definition, the undirected SCI can take values between 0 and 1, and the SCI of all states should sum up to 1. However, the index cannot resolve if the contribution of a state to the global effect is positive or negative (i.e., some states may show an effect opposite to the global effect thus reducing it overall). By including the sign of the effect of the state in question, we can obtain a directed measure of the state contribution:

$$SCI_{directed} = \frac{Effect^{(k)}}{\sum_{k=1}^{K} |Effect_k|}$$

The index can take values between -1 and 1, where positive values indicate a positive contribution of the state to the global effect, while negative values indicate a negative contribution of the state. Due to the possible changes in signs, the directed SCIs across states are not guaranteed sum up to 1 and the obtained values are only informative in terms of the direction and relative strength of the contribution of a state to the global effect, but the values cannot be interpreted in terms of a proportion of effect contributed by the state.

2.4.5. Statistical analyses

The power change in the α-band (IAF ± 2 Hz) with respect to baseline, averaged over all 42 ROIs, as well as the change in fractional occupancy and other state characteristics (dwell times, interval times) were assessed using repeated measures ANOVAs with factors STIMULATION (2-levels, tACS vs. sham, dataset 1: between-subject, dataset 2: within-subject) and STATE (4-levels, within-subject in both datasets). Greenhouse-Geisser corrected p-values are reported if sphericity was violated. Partial η^2 is reported as a measure of effect size:

$$\eta^2 = \frac{SS_{nominator}}{SS_{nominator} + SS_{demominator}}$$

To resolve in which states tACS led to a larger power increase relative to baseline as compared to sham, relative power changes in each state of all 42 ROIs were submitted to non-parametric random permutation cluster t-tests (two-sided; dataset 1: independent samples, dataset 2: dependent samples), using 10,000 randomizations and Monte-Carlo estimates for p-values. The obtained p-values were Bonferroni-corrected for the 4 multiple comparisons in addition to the cluster correction within each test.

3. Results

3.1. HMM decomposes time-series into transient states

The HMMs decomposed the source time-series into brain-states with distinct spatial, spectral and connectivity profiles. In an initial step, we tested different HMMs with the number of states ranging from two to twelve. After inspection of the results, we decided to settle for a four-state HMM for subsequent analyses, as it returned distinct brain-states without producing redundant (i.e., two or more similar) states (see Supplementary Fig. 4 for an example). The states seem to correspond to sensori-motor, visual, and default mode network (DMN) states as well a negative activation state (relative to the other states; Fig. 3) and seem generally in agreement with previous work (Vidaurre et al., 2018b). However, while the more complex 12-state HMM in Vidaurre et al. revealed an anterior and a posterior sub-network of the DMN, our 4-state model seemed to have returned a general DMN state, somewhat similar to the combination of the anterior and posterior higher-order cognitive state described by the authors (compare Fig. 6 in Vidaurre et al., 2018b). Of note, the authors also find several "negative activation" states, similar to what we observe in state 1.

3.2. tACS differentially affects α-power across states, but not state occupancy

To test if tACS differentially affected brain-states, we compared the power increase in the individual α-band (IAF ± 2 Hz) relative to baseline, averaged over all 42 ROIs, between the tACS and the sham group using a repeated measures ANOVA with the within-subject factor STATE (4-levels) and the between-subject factor STIMULATION (2-levels; tACS vs. sham). Results yielded significant main effects of STIMULATION ($F_{1,38} = 9.61$, $p = .0036$, $\eta^2 = 0.13$) and STATE ($F_{3,114} = 6.28$, $p = .008$, $\eta^2 = 0.06$) and a significant STIMULATION*STATE interaction ($F_{3,114} = 4.28$, $p = .031$, $\eta^2 = 0.04$), indicating that the tACS effect differed across spontaneous brain-states (Fig. 4a, b).

To assess which states were affected by stimulation, we subsequently performed two-sided non-parametric random permutation cluster t-tests for independent samples comparing the power increase following tACS and sham in each state. Tests yielded a significant cluster in state 2 ($p_{cluster} = .0012$, df = 38, Fig. 4c). No clusters were identified in the other states (all $p_{cluster} > .14$, all df = 38, Supplementary Table 1). We did not find evidence for effects of tACS in the neighboring θ- (IAF-7 Hz – IAF-3 Hz) and β-bands (IAF + 4 Hz – IAF + 20 Hz; Supplementary Table 2). When we repeated the analysis for HMMs with other numbers of states ($k = 2$ to $k = 12$) we obtained similar results, i.e., tACS consistently affected a single state that showed activation and connectivity patterns very similar to the DMN state in the 4-state HMM (see Supplementary Fig. 5 for exemplary results for the 6-state model).

To test whether tACS affects the time spent in each state (a.k.a. the fractional occupancy), we compared the absolute change in fractional occupancy from baseline to post-stimulation between tACS and sham using a repeated measures ANOVA with the within-subject factor STATE (4-levels) and the between-subject factor STIMULATION (2-levels; tACS vs. sham). The analysis yielded a significant main effect of STATE ($F_{3,114} = 4.17$, $p = .024$, $\eta^2 = 0.09$), indicative of a general change of fractional occupancy across states, but neither an effect of STIMULATION ($F_{1,38} < 0.01$, $p = 1$, $\eta^2 < 0.01$), nor a STIMULATION*STATE interaction ($F_{3,114} = 1.70$, $p = .25$, $\eta^2 = 0.04$), suggesting that tACS did not influence the occurrence of transient states (Fig. 4d).

We next assessed if tACS influenced the duration of individual state visits (dwell times) or the time between visits to the same state. To this end, we submitted the absolute change in dwell and interval times to two repeated measures ANOVAs with between subject factor STIMULATION and within subject factor STATE. While there was a significant main effect of STATE ($F_{3,114} = 11.89$, $p < .001$, $\eta^2 = 0.13$) on participants dwell times, we did not observe any main effect of STIMULATION ($F_{1,38} = 0.01$, $p = .91$, $\eta^2 < 0.01$) or a STIMULATION x STATE interaction ($F_{3,114} = 0.82$, $p = .49$, $\eta^2 = 0.01$) on dwell times. Neither main effects of STIMULATION ($F_{1,38} = 0.03$, $p = .86$, $\eta^2 < 0.01$) or STATE ($F_{3,114} = 1.60$, $p = .21$, $\eta^2 = 0.03$), nor an interaction effect of STIMULATION x STATE ($F_{3,114} = 0.16$, $p = .77$, $\eta^2 < 0.01$) were observed with respect to changes in state interval times.

3.3. Results replicate in validation data

The HMM analysis on the second dataset returned states with spatio-spectral profiles similar to the ones obtained in the first dataset (Fig. 5).

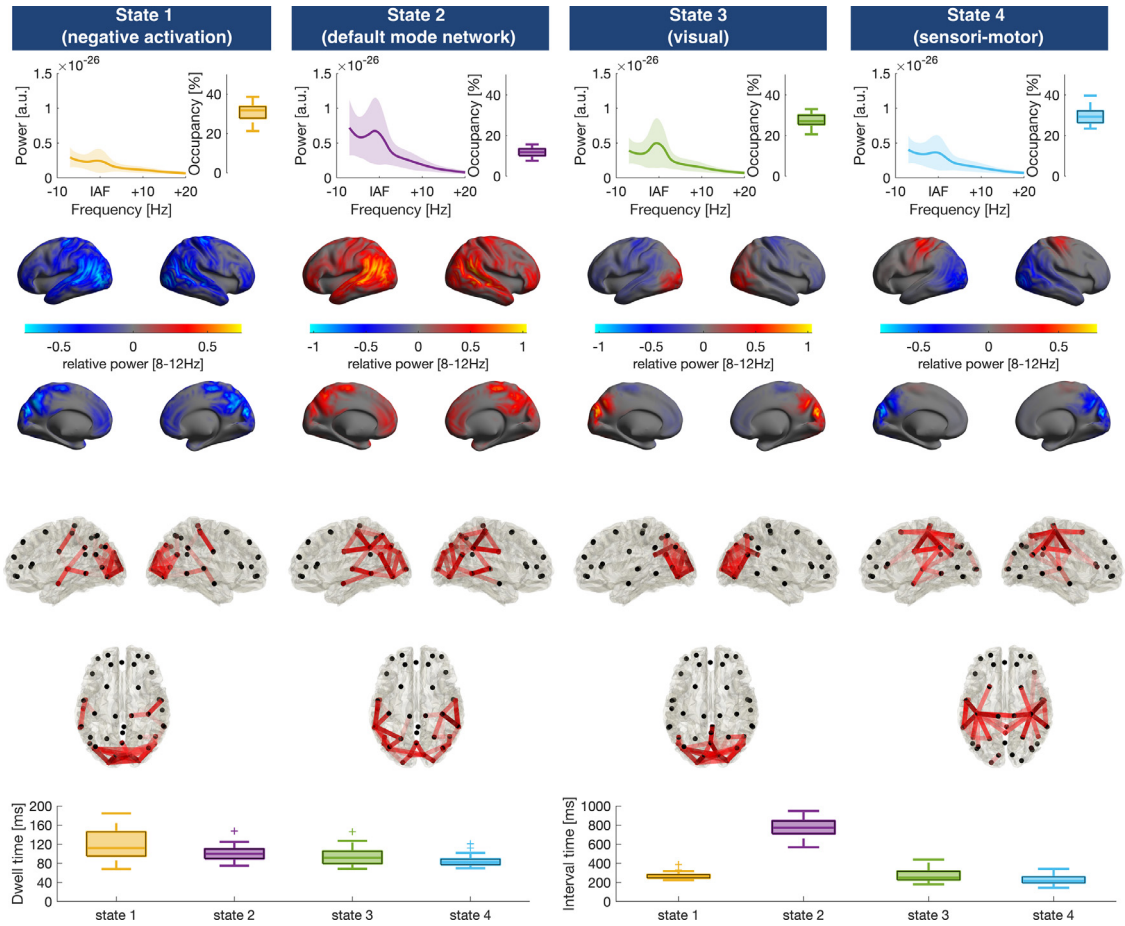

Fig. 3. *State profiles in experiment 1.* Each column depicts power spectra, relative state occupancy (top row), spatial maps of α-power relative to the average over all states (1st middle row) and connectivity profiles (2nd middle row, coherence in the α-band) for each of the four states. Connectivity profiles are thresholded to show the 5% strongest connections, darker shades of red indicate higher connection strength. Shaded areas depict standard deviation (S.D.). Bottom row depicts dwell times (average time a state is active during each visit; left column) and interval times (average time between visits to a state; right column) of each of the states.

Like our results in the first dataset, the states seem to reflect visual, sensori-motor and DMN activity as well as a negative activation state.

Again, we assessed the effect of tACS on power in the individual α-band (IAF $\pm$ 2 Hz) using a repeated measures ANOVA with the within-subject factors STIMULATION (2-levels; tACS vs. sham) and STATE (4-levels). The analysis yielded significant effects of STIMULATION ($F_{1,18} = 9.06$, $p = .008$, $\eta^2 = 0.06$) and STATE ($F_{3,54} = 5.05$, $p = .013$, $\eta^2 = 0.02$). Importantly, the STIMULATION*STATE interaction again reached significance ($F_{3,54} = 6.88$, $p = .004$, $\eta^2 = 0.02$), replicating the differential effect of tACS across states found in the first dataset (Fig. 6a, b). To assess which states were affected by stimulation, we subsequently performed two-sided non-parametric random permutation cluster t-tests for dependent samples comparing the power increase during stimulation and sham in each state. Tests yielded a significant cluster in state 4 ($p_{cluster} = .004$, df = 18, Fig. 6c) as well as a trend in state 3 ($p_{cluster} = .07$, df = 18, trend not shown in cluster maps). No effects were found in the other states (all $p_{cluster} > .46$, df = 18, Supplementary Table 3). Noteworthy, state 4 in this dataset shows strong similarities with state 2 from dataset 1 (Fig. 3 second column, Fig. 5 fourth column), which was the only state showing a significant effect to tACS in the previous analysis (Fig. 4). Again, we did not find evidence for effects of tACS in the neighboring θ- (IAF-7 Hz – IAF-3 Hz) and β-band (IAF + 4 Hz – IAF + 20 Hz; Supplementary Table 4).

We next assessed whether tACS affected the time spent in each state by submitting the absolute change in fractional occupancy from baseline to the post-stimulation period to a repeated-measures ANOVA with the within subject factors STIMULATION (2-levels, tACS vs. sham) and STATE (4-levels). Once again, the analysis revealed a significant effect of STATE ($F_{3,54} = 10.25$, $p < .001$, $\eta^2 = 0.21$), but neither a main effect of STIMULATION ($F_{1,18} < 0.01$, $p = 1$, $\eta^2 < 0.01$), nor a STIMULATION*STATE interaction ($F_{3,54} = 1.07$, $p = .33$, $\eta^2 = 0.03$), suggesting that tACS did not affect the relative time spent in each of the states (Fig. 6d).

We subsequently tested if tACS influenced the duration of individual state visits (dwell times) or the time between visits to the same state. To this end, we submitted the absolute change in dwell and interval times to two repeated measures ANOVAs with within subject factors STATE and STIMULATION. While there was a significant main effect of STATE on participants dwell ($F_{3,54} = 9.14$, $p < .001$, $\eta^2 = 0.18$) and interval times ($F_{3,54} = 2.86$, $p = .045$, $\eta^2 = 0.07$), we did not observe any main effect of STIMULATION (dwell times: $F_{1,18} = 3.66$, $p = .07$, $\eta^2 = 0.03$; interval times: $F_{1,18} < 0.01$, $p = .94$, $\eta^2 < 0.01$) or a STIMULATION x STATE interaction (dwell times: $F_{3,54} = 2.35$, $p = .08$, $\eta^2 = 0.04$; interval times: $F_{3,54} = 1.84$, $p = .15$, $\eta^2 = 0.04$) on either of the measures.

3.4. DMN state disproportionally drives global tACS effect

Our results so far suggest that one out of our four transient brain-states is most susceptible to tACS. But does this state also drive the tACS effect on a global level? To address this question, we revisited the global (i.e., non-state-solved) tACS effect in the within-subject dataset. We computed non-state-resolved power spectra from our ROI time se-

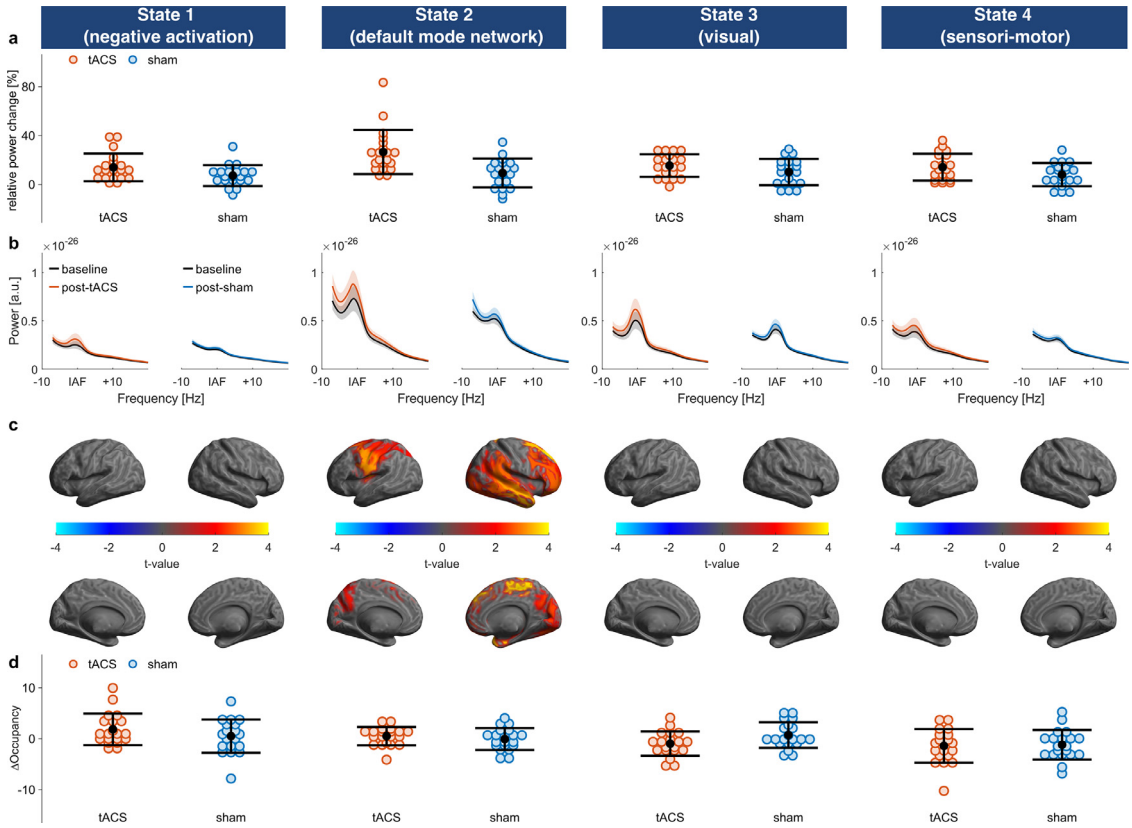

Fig. 4. *State-specific tACS effect in experiment 1.* (a) Relative power change per state in the two experimental groups (tACS vs. sham). Black dots and error bars indicate mean and S.D. Colored dots indicate the distribution of individual datapoints. (b) Average power spectra over all ROIs before and after tACS or sham stimulation, respectively. Shaded areas depict standard error of the mean (S.E.M.) (c) Significant clusters exhibiting larger relative power increase in the α-band after tACS as compared to sham stimulation. *T*-value maps are thresholded at an α-level of 0.05 (after an additional Bonferroni correction for four multiple comparisons). Only one of the four states (state 2) was susceptible to tACS. (d) Change in fractional occupancy per state for the two experimental sessions (tACS vs. sham). TACS did not change the relative occurrence of states compared to sham.

ries and computed the pre- to post-stimulation power increase in the individual α-band and submitted the resulting data to a dependent samples random-permutation cluster test. The test confirmed a global effect of tACS in the data ($p_{cluster}$ = .006, df = 18; Fig. 7a–c). Importantly, the global cluster shows a substantial spatial overlap with the cluster found in the DMN state (state 4) in the second dataset, with 12 out of 18 significant ROIs in the global cluster overlapping (Fig. 7d).

We next estimated how much of the effect seen at the global level can be attributed to each of the transient brain-states. To this end, we computed the directed and undirected state contribution indices as detailed in Section 2.4.4. In short, the indices estimate the relative contribution of the tACS effect in each state to the global effect, taking into account the state probability series. The $SCI_{undirected}$ provides an estimate of the proportion of the overall tACS related α-power dynamics explained by each state, irrespective of its direction. The $SCI_{undirected}$ estimates the relative contribution between states, taking into account whether the state makes a positive or negative contribution to the global tACS effect.

Our results suggest, that while the DMN state occupies only M = 12.73% (SD = 2.52) of the overall experiment time (Fig. 5 top), it on average, contributes M = 31.02% (SD = 10.38) to the global tACS related α-power dynamics (Fig. 7e). In contrast, each of the remaining 3 states occupies around 29% of the overall experiment time, while only contributing 20–25% to the overall dynamics. $SCI_{undirected}$ in the DMN state was significantly larger as compared to the average across the remaining states (t_{18} = 2.53, p = .02). Further, the DMN state was the only state showing a net positive directed contribution to the global effect, significantly different from zero (t_{18} = 3.41, $p_{Bonferroni}$ = 0.013; Fig. 7f). None of the other states showed a significant directed contribution (all p > .16, uncorrected). Similar to the $SCI_{undirected}$, $SCI_{directed}$ was significantly larger in the DMN state as compared to the average of the other states (t_{18} = 2.59, p = .02).

4. Discussion

In the current study, we aimed to reveal the role of hidden, spontaneous brain-state dynamics on aftereffects of tACS. To this end, we adapted a novel analysis framework to decompose neural time series data into brain-states using Hidden Markov Models (Baker et al., 2014; Vidaurre et al., 2018b, 2016). These states are characterized by distinct spatial, spectral and connectivity profiles and reflect known networks of human brain activity. The approach further allowed us to gain insights to the nature of changes underlying the increase in spectral power often associated with tACS (Kasten et al., 2016; Veniero et al., 2015; Zaehle et al., 2010). Our results suggest that tACS distinctly and consistently modulated α-power within the same state across both datasets, which we identified as most likely reflecting DMN activity. We did not find evidence for such an effect in other states. Further analyses in our within-subject dataset suggest that the effect in the DMN state substantially overlaps with the tACS effect seen on a global level and seems to be the most significant driving force of the global effect. This significant contribution of the state occurs despite the fact that the state is active for only ~12% of the total time. We did not find evidence that the time spent in any of the states was modulated by tACS, or that the stimulation gave rise to entirely new brain-states. Overall this finding confirms the general assumption that tACS indeed affects the power of oscillatory activity but not how frequently this activity occurs.

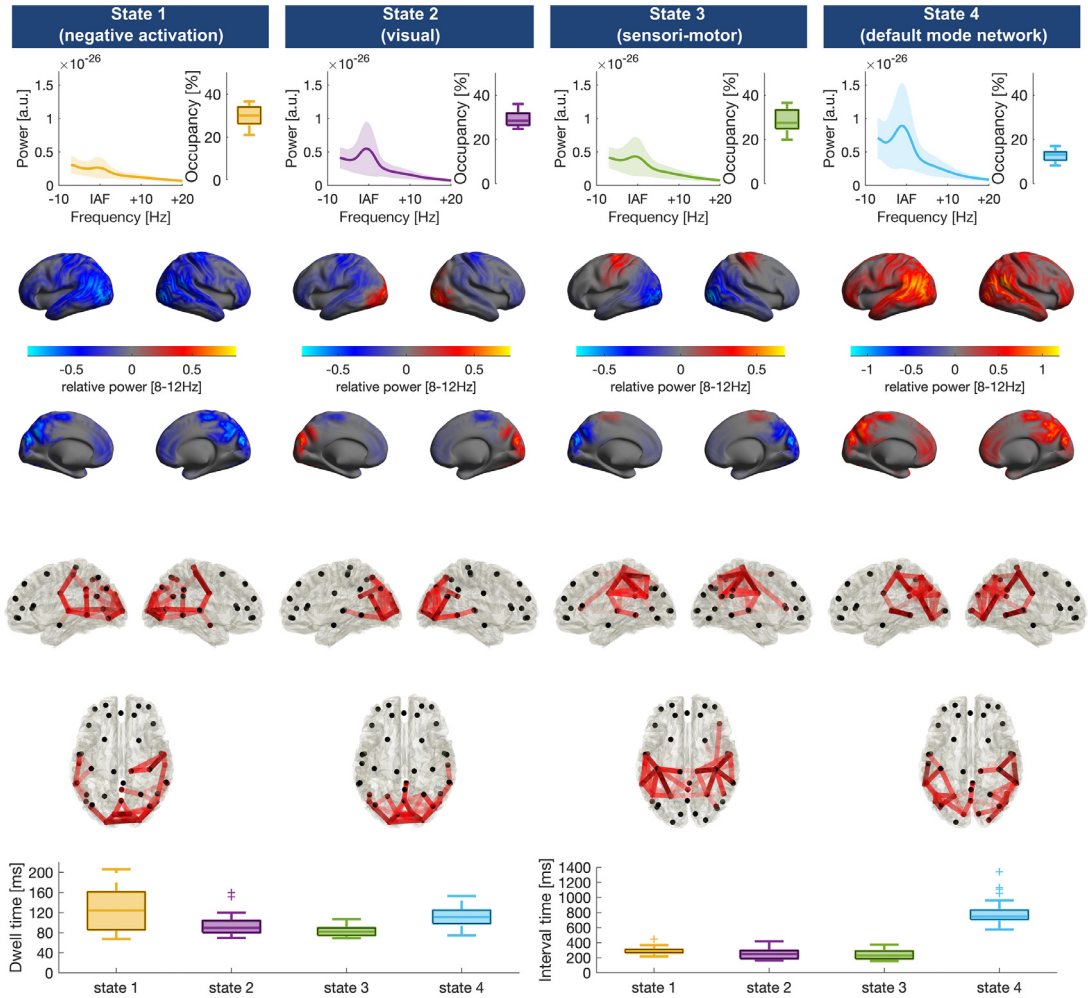

Fig. 5. *State profiles in experiment 2.* Each column depicts power spectra, relative state occupancy (top row), spatial maps of α-power relative to the average over all states (1st middle row) and connectivity profiles (2nd middle row, coherence in the α-band) for each of the four states. Connectivity profiles are thresholded to show the 5% strongest connections. Shaded areas depict standard deviation (S.D.). Bottom row depicts dwell times (average time a state is active during each visit; left column) and interval times (average time between visits to a state; right column) of each of the states.

TACS is generally considered a subthreshold stimulation approach. As such, it is believed to be capable of modulating pre-existing oscillatory activity, but not of inducing new oscillatory activity. In line with this idea, the state most affected by stimulation was one that shows considerable amounts of endogenous activity in the α-band. To our surprise, however, the state that captured visual α-oscillations, seemed to have not been affected by tACS, and seems to show the lowest contribution to the global tACS effect (Fig. 7f). The Cz-Oz montage used during the experiment was originally designed to maximize current in the occipital lobe (Neuling et al., 2012). This raises the question; which properties of a brain-state determine whether it is susceptible to tACS? For example, it has been suggested that states with already high oscillatory activity cannot be further elevated due to ceiling effects (Neuling et al., 2013; Ruhnau et al., 2016). Alternatively, it has been argued that at least some involvement of the target oscillation in the state is necessary for the stimulation to elicit effects (Feurra et al., 2013; Kasten and Herrmann, 2017). Unfortunately, neither of these explanations can fully account for our findings of a susceptible, high α-power DMN state and an unsusceptible high α-power visual state. This may indicate that our current perspectives on the state-dependency of tACS effects may be too simplistic. To what extent other features of brain-states such as the number of brain regions involved, their connectivity profiles, the duration for which the state is active, the nature of the underlying information processing or subtle differences in the underlying activity patterns might play a role remains largely elusive and may deserve consideration in future studies. Noteworthy, the DMN state most affected by tACS in both datasets happens to be the state that was active for the least amount of time, while exhibiting the most widespread activation and connectivity profile. Previous studies have linked posterior α-oscillations with DMN functioning (Knyazev et al., 2011; Mo et al., 2013). In particular, a recent study demonstrated that α-tACS applied to the occipito-parietal midline did not only increase the power of intrinsic α-oscillations, but also caused an upregulation of DMN connectivity (Clancy et al., 2022).

The differential effect of tACS on spontaneous brain-states has implications for the variability of stimulation effects. As illustrated in Fig. 1, changes in the time spent in the brain-state susceptible to stimulation may obscure stimulation effects. Although we did not find evidence that tACS induces such changes in our data, it may be possible that they may occur at random or due to factors unrelated to stimulation (e.g., fatigue/time on task, context conditions, experimental manipulations, etc.). Another aspect that may be worth considering, is the effective stimulation duration that may follow from our results. The susceptible brain-state is active for approximately 10–15% of the recording time. Assuming that the state dynamics *during* tACS remain comparable to those before and after stimulation, and that tACS only exerts its effects during the time the susceptible state is active, this would imply that our 20 min period of tACS may have contained less than 3 min of effective stimulation. It should be emphasized, though, that these consider-

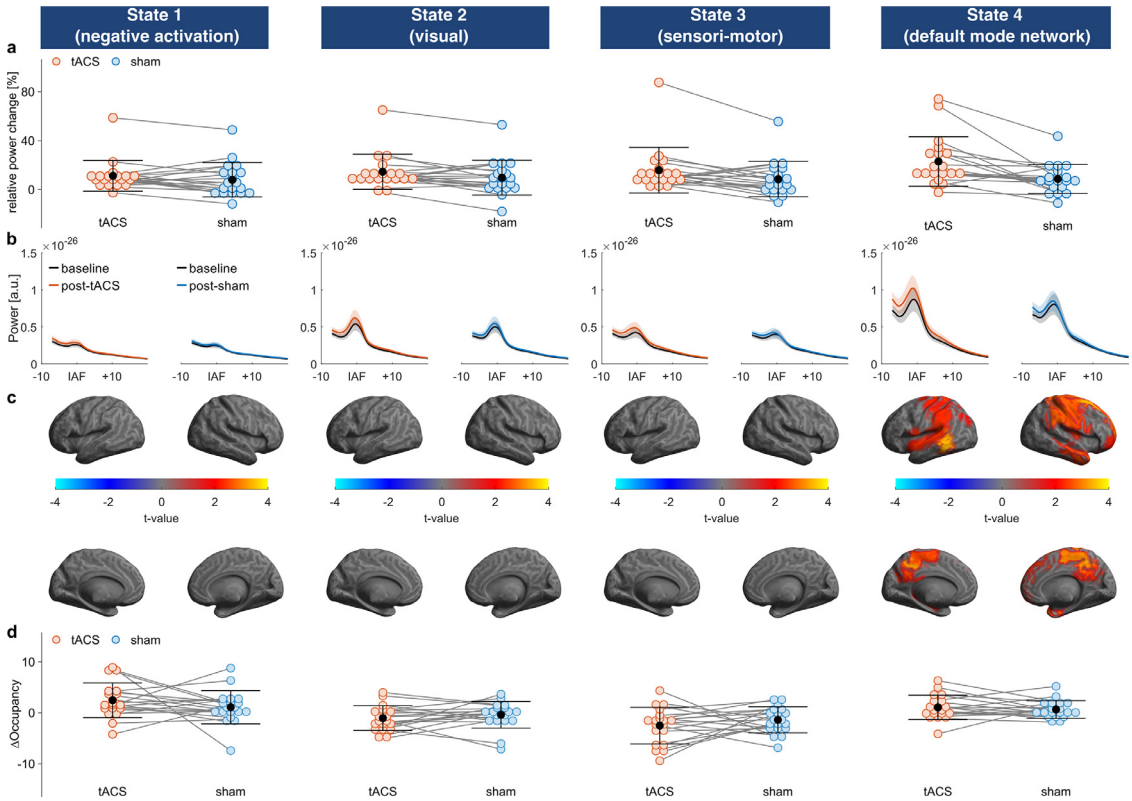

Fig. 6. *State-specific tACS effect in experiment 2.* (a) Relative power change per state in the two experimental groups (tACS vs. sham). Black dots and error bars indicate mean and S.D. Colored dots indicate the distribution of individual datapoints. Gray lines indicate within subject differences between stimulation sessions. (b) Average power spectra over all ROIs before and after tACS or sham stimulation, respectively. Shaded areas depict standard error of the mean (S.E.M.). (c) Significant clusters exhibiting larger relative power increase in the α-band after tACS as compared to sham stimulation. *T*-value maps are thresholded at an α-level of 0.05 (after Bonferroni correction for four multiple comparisons). Only one of the four states (state 4) appeared to be susceptible to tACS. (d) Change in fractional occupancy per state for the two experimental sessions (tACS vs. sham). TACS did not change the relative occurrence of states compared to sham.

ations are highly speculative as the HMM approach cannot be reliably applied during stimulation due to the contamination of MEG signals with a large electromagnetic artifact which are notoriously difficult to remove (Gebodh et al., 2019; Kasten et al., 2018a, 2018b; Neuling et al., 2017; Noury et al., 2016; Noury and Siegel, 2018, 2017, for an overview see Kasten and Herrmann 2019).

Some limitations of the current study and its methodology deserve discussion. The HMM requires the user to pre-specify the number of states to be found in the data. In our analysis we settled for a four state HMM, as larger numbers resulted in a certain redundancy (i.e., similarity between two or more states) of the states returned by the model. This does, however, not imply that the brain exclusively switches between these four states. Specifying a larger number of states, may be useful depending on the specific research question, e.g., if a more fine-grained decomposition of states is desired. For example, using a 12-state HMM could be used to identify subnetworks of the DMN (Vidaurre et al., 2018b). However, such more detailed descriptions of the data come at the cost of a larger number of multiple comparisons that have to be taken into account and may hamper statistical power. In addition, an overall more complex pattern of results may be more difficult to interpret.

The results at hand were obtained from a re-analysis of two existing datasets (Kasten et al., 2019). Consequently, the current results cannot be interpreted as an independent replication of the aftereffect of tACS, but rather provides a different point of view on the underlying tACS-induced oscillatory changes already demonstrated in this dataset. Further, the datasets only provide data for one stimulation montage and frequency along with a sham control. This precludes definitive conclusions about the frequency specificity of tACS and how it might relate to brain-state dynamics based on the current findings. It is generally believed that tACS elicits its effects in a frequency specific manner, i.e. only modulates oscillations within the frequency band at which it is applied. Indeed several studies report frequency specific effects of stimulation on behavioral tasks or MEP measures (Feurra et al., 2013; Kasten et al., 2020; Wöstmann et al., 2018). Testing frequency specificity in the context of tACS aftereffects is however challenging and time consuming, as each additional stimulation condition (i.e., frequency) included in the protocol requires an additional recording session (or experimental group) increasing the burden of measurements for both participants and experimenters. We therefore refrained from including more stimulation conditions when the data was originally acquired. While the state-dependent effect of our α-tACS seems to be limited to the α-band, it cannot be ruled out that stimulation at other frequencies would have had the same effect. TACS at other stimulation frequencies could for example modulate oscillations in the α-band via entrainment of harmonic frequencies (Herrmann, 2001; Herrmann et al., 2016a), cross-frequency interactions (Boyle and Frohlich, 2013; Palva, 2005) or via unintended side effects, such as stimulation of peripheral nerves that could give rise to changes in arousal or vigilance (Schutter, 2016, but see Kasten et al. 2019). In addition, it remains elusive how such stimulation would have interacted with the different brain-states. One could for example speculate that different states and their underlying networks might be susceptible to stimulation at different frequencies. Future studies adapting the HMM approach to experiments with different stimulation protocols are thus desirable to better generalize the current findings. Those studies could, for example, apply stimulation montages to specifically target each of the states reported here and differentially test their susceptibility to stimulation. For the current study, we aimed to establish the existence of differential responses to tACS across transient brain-states, which is,

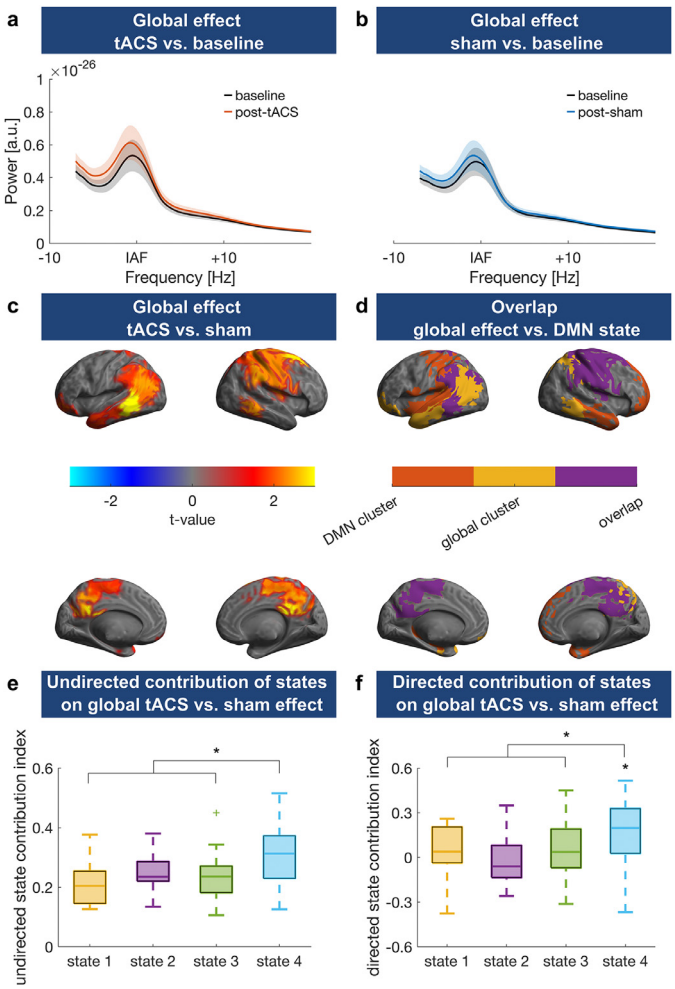

Fig. 7. *Global vs. brain-state resolved tACS effect in within-subject data.* (a, b) Spectra depict the global (non- state-resolved) power increase across all ROIs from the pre- to the post stimulation periods for the tACS (a) and sham (b) condition. Shaded areas indicate S.E.M. (c) Significant clusters exhibiting a larger α-power increase after tACS as compared to sham. T-value map is thresholded at an α-level of 0.05. (d) Cluster overlap between global tACS effect and the effect observed in the DMN state in experiment 2. (e, f) Relative contribution of the tACS effect within each state on the global tACS effect. (e) Undirected contribution of each state, indexing the proportion of the overall global dynamics explained by the state. (f) Directed contribution of each state. Positive values indicate a positive contribution to the global effect, while negative values indicate a negative influence of the state on the global effect. Asterisks indicate significant differences (* $p < .05$).

to some degree, independent from the question of whether or not effects of tACS are frequency specific. Even in the (hypothetical) case that tACS would be demonstrated to have effects on α-oscillations that are independent of stimulation frequency, such a finding would not render the observation of a differential effect of tACS across transient brain-states invalid. Another interesting application of HMMs in the context of tACS effects may additionally lie in the combination with cognitive tasks. Given a sufficiently large number of states, HMMs may allow to uncover which subprocess of a task is affected by stimulation. This may foster our understanding of how tACS exerts its behavioral effect, or to even tailor stimulation more specifically to target such subprocesses spatially, temporally and in terms of frequency thereby improving the capabilities of neuroimaging informed brain stimulation (Bergmann, 2018; Bergmann et al., 2016).

In general, HMMs may have a wide range of applications in the research of non-invasive brain stimulation. Their usage is not limited to M/EEG signals, but they can be utilized in any neuroimaging modality. For example its application to fMRI (Baker et al., 2014) might be particularly interesting to study spontaneous state dependency of tDCS. HMMs thus offer a versatile tool to uncover hidden dynamics behind brain stimulation effects and could foster our understanding of brain-state-dependency by providing a more detailed view on neuroimaging data of brain stimulation experiments.

Data availability

ROI time series, along with the underlying MATLAB code of this work are available via the open science framework: https://osf.io/8cyt6/ (dataset 1) and https://osf.io/btwgy/ (dataset 2). Raw-MEG data and structural MRIs are available upon reasonable request from the corresponding author CSH. Raw data are not publicly available due to potentially identifying information that could compromise participant privacy.

Declaration of Competing Interest

CSH holds a patent on brain stimulation. FHK, declares no competing interests.

Credit authorship contribution statement

Florian H. Kasten: Conceptualization, Methodology, Software, Formal analysis, Investigation, Writing – original draft, Visualization. **Christoph S. Herrmann:** Writing – review & editing, Supervision, Funding acquisition.

Data availability

The data is available - links are in the manuscript.

Acknowledgments

This research was supported by the Neuroimaging Unit of the Carl von Ossietzky University Oldenburg funded by grants of from the German Research Foundation (3T MRI INST 184/152-1 FUGG and MEG INST 184/148-1 FUGG). Christoph S. Herrmann was supported by a grant of the German Research Foundation (Deutsche Forschungsgemeinschaft, DFG) under Germany's Excellence Strategy – EXC 2177/1 - Project ID 390895286.

Supplementary materials

Supplementary material associated with this article can be found, in the online version, at doi:10.1016/j.neuroimage.2022.119713.

References

Alagapan, S., Schmidt, S.L., Lefebvre, J., Hadar, E., Shin, H.W., Fröhlich, F., 2016. Modulation of cortical oscillations by low-frequency direct cortical stimulation is state-dependent. PLoS Biol. 14, e1002424. doi:10.1371/journal.pbio.1002424.

Alexander, M.L., Alagapan, S., Lugo, C.E., Mellin, J.M., Lustenberger, C., Rubinow, D.R., Fröhlich, F., 2019. Double-blind, randomized pilot clinical trial targeting alpha oscillations with transcranial alternating current stimulation (tACS) for the treatment of major depressive disorder (MDD). Transl. Psychiatry 9, 106. doi:10.1038/s41398-019-0439-0.

Baker, A.P., Brookes, M.J., Rezek, I.A., Smith, S.M., Behrens, T., Probert Smith, P.J., Woolrich, M., 2014. Fast transient networks in spontaneous human brain activity. eLife 3, e01867. doi:10.7554/eLife.01867.

Baum, L.E., Petrie, T., Soules, G., Weiss, N., 1970. A Maximization technique occurring in the statistical analysis of probabilistic functions of Markov chains. Ann. Math. Stat. 41, 164–171. doi:10.1214/aoms/1177697196.

Bergmann, T.O., 2018. Brain state-dependent brain stimulation. Front. Psychol. 9. doi:10.3389/fpsyg.2018.02108.

Bergmann, T.O., Hartwigsen, G., 2020. Inferring causality from noninvasive brain stimulation in cognitive neuroscience. J. Cogn. Neurosci. 1–12. doi:10.1162/jocn_a_01591.

Bergmann, T.O., Karabanov, A., Hartwigsen, G., Thielscher, A., Siebner, H.R., 2016. Combining non-invasive transcranial brain stimulation with neuroimaging and electrophysiology: current approaches and future perspectives. Neuroimage 140, 4–19. doi:10.1016/j.neuroimage.2016.02.012.

Boyle, M.R., Frohlich, F., 2013. EEG feedback-controlled transcranial alternating current stimulation. In: Procedings of the 6th International IEEE/EMBS Conference on Neural Engineering (NER), San Diego, CA, USA. IEEE, pp. 140–143. doi:10.1109/NER.2013.6695891 Presented at the 2013 6th International IEEE/EMBS Conference on Neural Engineering (NER).

Clancy, K.J., Andrzejewski, J.A., You, Y., Li, W., 2022. Transcranial stimulation of alpha oscillations up-regulates the default mode network. Proc. Natl. Acad. Sci. 119. doi:10.1073/pnas.2110868119.

Colclough, G.L., Brookes, M.J., Smith, S.M., Woolrich, M.W., 2015. A symmetric multivariate leakage correction for MEG connectomes. Neuroimage 117, 439–448. doi:10.1016/j.neuroimage.2015.03.071.

Elyamany, O., Leicht, G., Herrmann, C.S., Mulert, C., 2020. Transcranial alternating current stimulation (tACS): from basic mechanisms towards first applications in psychiatry. Eur. Arch. Psychiatry Clin. Neurosci. doi:10.1007/s00406-020-01209-9.

Feurra, M., Blagovechtchenski, E., Nikulin, V.V., Nazarova, M., Lebedeva, A., Pozdeeva, D., Yurevich, M., Rossi, S., 2019. State-dependent effects of transcranial oscillatory currents on the motor system during action observation. Sci. Rep. 9, 12858. doi:10.1038/s41598-019-49166-1.

Feurra, M., Pasqualetti, P., Bianco, G., Santarnecchi, E., Rossi, A., Rossi, S., 2013. State-dependent effects of transcranial oscillatory currents on the motor system: what you think matters. J. Neurosci. 33, 17483–17489. doi:10.1523/JNEUROSCI.1414-13.2013.

Fröhlich, F., McCormick, D.A., 2010. Endogenous electric fields may guide neocortical network activity. Neuron 67, 129–143. doi:10.1016/j.neuron.2010.06.005.

Gebodh, N., Esmaeilpour, Z., Adair, D., Chelette, K., Dmochowski, J., Woods, A.J., Kappenman, E.S., Parra, L.C., Bikson, M., 2019. Inherent physiological artifacts in EEG during tDCS. Neuroimage 185, 408–424. doi:10.1016/j.neuroimage.2018.10.025.

Herrmann, C.S., 2001. Human EEG responses to 1-100 Hz flicker: resonance phenomena in visual cortex and their potential correlation to cognitive phenomena. Exp. Brain Res. 137, 346–353. doi:10.1007/s002210100682.

Herrmann, C.S., Murray, M.M., Ionta, S., Hutt, A., Lefebvre, J., 2016a. Shaping intrinsic neural oscillations with periodic stimulation. J. Neurosci. 36, 5328–5337. doi:10.1523/JNEUROSCI.0236-16.2016.

Herrmann, C.S., Rach, S., Neuling, T., Strüber, D., 2013. Transcranial alternating current stimulation: a review of the underlying mechanisms and modulation of cognitive processes. Front. Hum. Neurosci. 7. doi:10.3389/fnhum.2013.00279.

Herrmann, C.S., Strüber, D., Helfrich, R.F., Engel, A.K., 2016b. EEG oscillations: from correlation to causality. Int. J. Psychophysiol. 103, 12–21. doi:10.1016/j.ijpsycho.2015.02.003.

Horvath, J.C., Forte, J.D., Carter, O., 2015a. Evidence that transcranial direct current stimulation (tDCS) generates little-to-no reliable neurophysiologic effect beyond MEP amplitude modulation in healthy human subjects: a systematic review. Neuropsychologia 66, 213–236. doi:10.1016/j.neuropsychologia.2014.11.021.

Horvath, J.C., Forte, J.D., Carter, O., 2015b. Quantitative review finds no evidence of cognitive effects in healthy populations from single-session transcranial direct current stimulation (tDCS). Brain Stimul. 8, 535–550. doi:10.1016/j.brs.2015.01.400.

Johnson, L., Alekseichuk, I., Krieg, J., Doyle, A., Yu, Y., Vitek, J., Johnson, M., Opitz, A., 2020. Dose-dependent effects of transcranial alternating current stimulation on spike timing in awake nonhuman primates. Sci. Adv. 6, eaaz2747. doi:10.1126/sciadv.aaz2747.

Kasten, F.H., Dowsett, J., Herrmann, C.S., 2016. Sustained aftereffect of α-tACS lasts up to 70 min after stimulation. Front. Hum. Neurosci. 10. doi:10.3389/fnhum.2016.00245.

Kasten, F.H., Duecker, K., Maack, M.C., Meiser, A., Herrmann, C.S., 2019. Integrating electric field modeling and neuroimaging to explain inter-individual variability of tACS effects. Nat. Commun. 10, 5427. doi:10.1038/s41467-019-13417-6.

Kasten, F.H., Herrmann, C.S., 2020. Discrete sampling in perception via neuronal oscillations—evidence from rhythmic, non-invasive brain stimulation. Eur. J. Neurosci. doi:10.1111/ejn.15006, n/a.

Kasten, F.H., Herrmann, C.S., 2019. Recovering brain dynamics during concurrent tACS-M/EEG: an overview of analysis approaches and their methodological and interpretational pitfalls. Brain Topogr. 32, 1013–1019. doi:10.1007/s10548-019-00727-7.

Kasten, F.H., Herrmann, C.S., 2017. Transcranial alternating current stimulation (tACS) enhances mental rotation performance during and after stimulation. Front. Hum. Neurosci. 11. doi:10.3389/fnhum.2017.00002.

Kasten, F.H., Maess, B., Herrmann, C.S., 2018a. Facilitated event-related power modulations during transcranial alternating current stimulation (tACS) revealed by concurrent tACS-MEG. eNeuro 5. doi:10.1523/ENEURO.0069-18.2018, ENEURO.0069-18.2018.

Kasten, F.H., Negahbani, E., Fröhlich, F., Herrmann, C.S., 2018b. Non-linear transfer characteristics of stimulation and recording hardware account for spurious low-frequency artifacts during amplitude modulated transcranial alternating current stimulation (AM-tACS). Neuroimage 179, 134–143. doi:10.1016/j.neuroimage.2018.05.068.

Kasten, F.H., Wendeln, T., Stecher, H.I., Herrmann, C.S., 2020. Hemisphere-specific, differential effects of lateralized, occipital–parietal α- versus γ-tACS on endogenous but not exogenous visual-spatial attention. Sci. Rep. 10, 12270. doi:10.1038/s41598-020-68992-2.

Klink, K., Paßmann, S., Kasten, F.H., Peter, J., 2020. The modulation of cognitive performance with transcranial alternating current stimulation: a systematic review of frequency-specific effects. Brain Sci. 10, 932. doi:10.3390/brainsci10120932.

Knyazev, G.G., Slobodskoj-Plusnin, J.Y., Bocharov, A.V., Pylkova, L.V., 2011. The default mode network and EEG alpha oscillations: an independent component analysis. Brain Res. 1402, 67–79. doi:10.1016/j.brainres.2011.05.052.

Krause, M.R., Vieira, P.G., Csorba, B.A., Pilly, P.K., Pack, C.C., 2019. Transcranial alternating current stimulation entrains single-neuron activity in the primate brain. Proc. Natl. Acad. Sci. USA 116, 5747–5755. doi:10.1073/pnas.1815958116.

Laakso, I., Tanaka, S., Koyama, S., De Santis, V., Hirata, A., 2015. Inter-subject variability in electric fields of motor cortical tDCS. Brain Stimul. 8, 906–913. doi:10.1016/j.brs.2015.05.002.

Lafon, B., Henin, S., Huang, Y., Friedman, D., Melloni, L., Thesen, T., Doyle, W., Buzsáki, G., Devinsky, O., Parra, L.C.A., Liu, A., 2017. Low frequency transcranial electrical stimulation does not entrain sleep rhythms measured by human intracranial recordings. Nat. Commun. 8, 1199. doi:10.1038/s41467-017-01045-x.

Maris, E., Oostenveld, R., 2007. Nonparametric statistical testing of EEG- and MEG-data. J. Neurosci. Methods 164, 177–190. doi:10.1016/j.jneumeth.2007.03.024.

Mellin, J.M., Alagapan, S., Lustenberger, C., Lugo, C.E., Alexander, M.L., Gilmore, J.H., Jarskog, L.F., Fröhlich, F., 2018. Randomized trial of transcranial alternating current stimulation for treatment of auditory hallucinations in schizophrenia. Eur. Psychiatr. 51, 25–33. doi:10.1016/j.eurpsy.2018.01.004.

Mo, J., Liu, Y., Huang, H., Ding, M., 2013. Coupling between visual alpha oscillations and default mode activity. Neuroimage 68, 112–118. doi:10.1016/j.neuroimage.2012.11.058.

Nenonen, J., Nurminen, J., Kičić, D., Bikmullina, R., Lioumis, P., Jousmäki, V., Taulu, S., Parkkonen, L., Putaala, M., Kähkönen, S., 2012. Validation of head movement correction and spatiotemporal signal space separation in magnetoencephalography. Clin. Neurophysiol. 123, 2180–2191. doi:10.1016/j.clinph.2012.03.080.

Neuling, T., Rach, S., Herrmann, C.S., 2013. Orchestrating neuronal networks: sustained after-effects of transcranial alternating current stimulation depend upon brain states. Front. Hum. Neurosci. 7. doi:10.3389/fnhum.2013.00161.

Neuling, T., Ruhnau, P., Weisz, N., Herrmann, C.S., Demarchi, G., 2017. Faith and oscillations recovered: on analyzing EEG/MEG signals during tACS. Neuroimage 147, 960–963. doi:10.1016/j.neuroimage.2016.11.022.

Neuling, T., Wagner, S., Wolters, C.H., Zaehle, T., Herrmann, C.S., 2012. Finite-element model predicts current density distribution for clinical applications of tDCS and tACS. Front. Psychiatry 3. doi:10.3389/fpsyt.2012.00083.

Nolte, G., 2003. The magnetic lead field theorem in the quasi-static approximation and its use for magnetoencephalography forward calculation in realistic volume conductors. Phys. Med. Biol. 48, 3637–3652. doi:10.1088/0031-9155/48/22/002.

Noury, N., Hipp, J.F., Siegel, M., 2016. Physiological processes non-linearly affect electrophysiological recordings during transcranial electric stimulation. Neuroimage 140, 99–109. doi:10.1016/j.neuroimage.2016.03.065.

Noury, N., Siegel, M., 2018. Analyzing EEG and MEG signals recorded during tES, a reply. Neuroimage 167, 53–61. doi:10.1016/j.neuroimage.2017.11.023.

Noury, N., Siegel, M., 2017. Phase properties of transcranial electrical stimulation artifacts in electrophysiological recordings. Neuroimage 158, 406–416. doi:10.1016/j.neuroimage.2017.07.010.

Oldfield, R.C., 1971. The assessment and analysis of handedness: the Edinburgh inventory. Neuropsychologia 9, 97–113. doi:10.1016/0028-3932(71)90067-4.

Oostenveld, R., Fries, P., Maris, E., Schoffelen, J.M., 2011. FieldTrip: open source software for advanced analysis of MEG, EEG, and invasive electrophysiological data. Comput. Intell. Neurosci. 2011, 1–9. doi:10.1155/2011/156869.

Palva, J.M., 2005. Phase synchrony among neuronal oscillations in the human cortex. J. Neurosci. 25, 3962–3972. doi:10.1523/JNEUROSCI.4250-04.2005.

Pohle, J., Langrock, R., van Beest, F.M., Schmidt, N.M., 2017. Selecting the number of states in hidden markov models: pragmatic solutions illustrated using animal movement. JABES 22, 270–293. doi:10.1007/s13253-017-0283-8.

Quinn, A.J., van Ede, F., Brookes, M.J., Heideman, S.G., Nowak, M., Seedat, Z.A., Vidaurre, D., Zich, C., Nobre, A.C., Woolrich, M.W., 2019. Unpacking transient event dynamics in electrophysiological power spectra. Brain Topogr. 32, 1020–1034. doi:10.1007/s10548-019-00745-5.

Reinhart, R.M.G., Nguyen, J.A., 2019. Working memory revived in older adults by synchronizing rhythmic brain circuits. Nat. Neurosci. 22, 820–827. doi:10.1038/s41593-019-0371-x.

Ridding, M.C., Ziemann, U., 2010. Determinants of the induction of cortical plasticity by non-invasive brain stimulation in healthy subjects: induction of cortical plasticity by non-invasive brain stimulation. J. Physiol. 588, 2291–2304. doi:10.1113/jphysiol.2010.190314.

Riddle, J., McPherson, T., Atkins, A.K., Walker, C.P., Ahn, S., Frohlich, F., 2020. Brain-derived neurotrophic factor (BDNF) polymorphism may influence the efficacy of tACS to modulate neural oscillations. Brain Stimul. 13, 998–999. doi:10.1016/j.brs.2020.04.012.

Ruhnau, P., Neuling, T., Fuscá, M., Herrmann, C.S., Demarchi, G., Weisz, N., 2016. Eyes wide shut: transcranial alternating current stimulation drives alpha rhythm in a state dependent manner. Sci. Rep. 6, 27138. doi:10.1038/srep27138.

Schutter, D.J.L.G., 2016. Cutaneous retinal activation and neural entrainment in transcranial alternating current stimulation: a systematic review. Neuroimage 140, 83–88. doi:10.1016/j.neuroimage.2015.09.067.

Taulu, S., Simola, J., 2006. Spatiotemporal signal space separation method for rejecting nearby interference in MEG measurements. Phys. Med. Biol. 51, 1759–1768. doi:10.1088/0031-9155/51/7/008.

Taulu, S., Simola, J., Kajola, M., 2005. Applications of the signal space separation method. IEEE Trans. Signal Process. 53, 3359–3372. doi:10.1109/TSP.2005.853302.

Van Veen, B.D., Van Drongelen, W., Yuchtman, M., Suzuki, A., 1997. Localization of brain electrical activity via linearly constrained minimum variance spatial filtering. IEEE Trans. Biomed. Eng. 44, 867–880. doi:10.1109/10.623056.

Veniero, D., Vossen, A., Gross, J., Thut, G., 2015. Lasting EEG/MEG aftereffects of rhythmic transcranial brain stimulation: level of control over oscillatory network activity. Front. Cell. Neurosci. 9. doi:10.3389/fncel.2015.00477.

Vidaurre, D., Abeysuriya, R., Becker, R., Quinn, A.J., Alfaro-Almagro, F., Smith, S.M.,

Woolrich, M.W., 2018a. Discovering dynamic brain networks from big data in rest and task. Neuroimage 180, 646–656. doi:10.1016/j.neuroimage.2017.06.077.

Vidaurre, D., Hunt, L.T., Quinn, A.J., Hunt, B.A.E., Brookes, M.J., Nobre, A.C., Woolrich, M.W., 2018b. Spontaneous cortical activity transiently organises into frequency specific phase-coupling networks. Nat. Commun. 9, 2987. doi:10.1038/s41467-018-05316-z.

Vidaurre, D., Quinn, A.J., Baker, A.P., Dupret, D., Tejero-Cantero, A., Woolrich, M.W., 2016. Spectrally resolved fast transient brain states in electrophysiological data. Neuroimage 126, 81–95. doi:10.1016/j.neuroimage.2015.11.047.

Vöröslakos, M., Takeuchi, Y., Brinyiczki, K., Zombori, T., Oliva, A., Fernández-Ruiz, A., Kozák, G., Kincses, Z.T., Iványi, B., Buzsáki, G., Berényi, A., 2018. Direct effects of transcranial electric stimulation on brain circuits in rats and humans. Nat. Commun. 9, 483. doi:10.1038/s41467-018-02928-3.

Vossen, A., Gross, J., Thut, G., 2015. Alpha power increase after transcranial alternating current stimulation at alpha frequency (α-tACS) reflects plastic changes rather than entrainment. Brain Stimul. 8, 499–508. doi:10.1016/j.brs.2014.12.004.

Vosskuhl, J., Strüber, D., Herrmann, C.S., 2018. Non-invasive brain stimulation: a paradigm shift in understanding brain oscillations. Front. Hum. Neurosci. 12, 211. doi:10.3389/fnhum.2018.00211.

Wischnewski, M., Engelhardt, M., Salehinejad, M.A., Schutter, D.J.L.G., Kuo, M.F., Nitsche, M.A., 2019. NMDA receptor-mediated motor cortex plasticity after 20 Hz transcranial alternating current stimulation. Cereb. Cortex 29, 2924–2931. doi:10.1093/cercor/bhy160.

Wöstmann, M., Vosskuhl, J., Obleser, J., Herrmann, C.S., 2018. Opposite effects of lateralised transcranial alpha versus gamma stimulation on auditory spatial attention. Brain Stimul. 11, 752–758. doi:10.1016/j.brs.2018.04.006.

Zaehle, T., Rach, S., Herrmann, C.S., 2010. Transcranial alternating current stimulation enhances individual alpha activity in human EEG. PLoS One 5, e13766. doi:10.1371/journal.pone.0013766.